PCCP

Accepted Manuscript

This is an *Accepted Manuscript*, which has been through the Royal Society of Chemistry peer review process and has been accepted for publication.

Accepted Manuscripts are published online shortly after acceptance, before technical editing, formatting and proof reading. Using this free service, authors can make their results available to the community, in citable form, before we publish the edited article. We will replace this *Accepted Manuscript* with the edited and formatted *Advance Article* as soon as it is available.

You can find more information about *Accepted Manuscripts* in the **Information for Authors**.

Please note that technical editing may introduce minor changes to the text and/or graphics, which may alter content. The journal's standard **Terms & Conditions** and the **Ethical guidelines** still apply. In no event shall the Royal Society of Chemistry be held responsible for any errors or omissions in this *Accepted Manuscript* or any consequences arising from the use of any information it contains.

Synthesis and characterization of π-conjugated copolymers with thieno-imidazole units in main chain: application for bulk heterojunction polymer solar cells

M. L. Keshtov[a*], D. Yu. Godovsky[a],   F. Ch. Chen[c] A. R. Khokhlov[a,b], S. A. Siddiqui[d], G. D. Sharma[d*]

[a]Institute of Organoelement Compounds of the Russian Academy of Sciences, Vavilova st., 28, 119991 Moscow, Russian Federation

[b]Lomonosov Moscow State University, Faculty of Physics, 1-2 Leninskiye Gory, Moscow,119991, Russian Federation.

[c] Department of Photonics, National Chiao Tung University, Hsinchu, Taiwan 300
[d] R & D Center for Engineering and Science, JEC group of Colleges, Jaipur Engineering College, Kukas, Jaipur 303101

Abstract

In this paper we describe the three new narrow bandgap D-A conjugated copolymers **P1**, **P2** and **P3** based on different weak donor fused thiophen-imidazol containing derivatives units and same benzothiadiazole acceptor unit were synthesized by Stille cross- coupling polymerization and were characterized by ^{1}H NMR, elemental analysis, GPC, TGA, DSC. These copolymers exhibit intensive absorbance in the range 350-900 nm and optical bandgap lies in the range of 1.50 -1.61 eV, which corresponds to the maximum photon flux of solar spectrum. The electrochemical bandgap derived from cyclic voltammetry varies within the limits 1.47- 1.65 eV and approximately well very close to the optical bandgap. The highest occupied molecular orbital (HOMO) energy level of all copolymers is deep lying (-5.24 eV and -5.37 eV and -5.25 eV for **P1, P2** and **P2**, respectively) which show that copolymers has good stability in the air and assured a higher open circuit voltage (V_{oc}) for polymer BHJ solar cells. These copolymer were used as donor along with $PC_{71}BM$ and the BHJ polymer solar cells based on **P1**:$PC_{71}BM$, **P2**:$PC_{71}BM$ and **P3**:$PC_{71}BM$ processed from chloroform (CF) solvent with 3 %v DIO as additive showed over all PCE of 4.55 %, 6.76 % and 5.16 %, respectively.

Key words: D-A copolymers, Bulk heterojunction solar cells, Power conversion efficiency, Solvent additives

Corresponding authors, E-mail: sharamgd_in@yahoo.com and gdsharma273@gmail.com (G. D. Sharma), keshtov@ineos.ac.ru (M. L. Keshtov)

1. Introduction

Organic solar cells (OSCs) have attracted remarkable attention in last two decades because of their advantages in low cost, roll to roll device fabrication, light weight and mechanical flexibility [1]. Among the all device architectures, OSCs based on bulk heterojunction (BHJ) active layer consist of a blend of electron donor (conjugated polymer or small molecules) and electron acceptor (fullerene derivatives), is one of the most promising options [2]. At present, state of the art OSCs have reached the power conversion efficiency (PCE) over 9 % for single junction devices [3] and as high as 10.6 % for tandem device [4]. Moreover, it is expected to reach 15 % in next few years [5] by developing new organic semiconductors, optimizing device architectures and under standing the device physics [6]. Theoretical suggest that the maximum PCE of the single layer polymer solar cells could be reached up to 17 % and that tandem PSCs have capability for a maximum PCE of 24 % [7].

The power conversion efficiency of BHJ polymer solar cells depends on the absorption profile and bandgap of the conjugated electron donor polymer used in the BHJ active layer. To explore novel electron donor conjugated polymeric materials to improve PCE of organic solar cells further, donor –acceptor (D-A) approach is one of the most successful strategies, because it enables tunable absorption spectra and tailor the electrochemical energy levels (highest occupied molecular orbital (HOMO) and lowest unoccupied molecular orbital (LUMO) energy levels) of resulting polymers [8]. Therefore it is essential to develop the D-A copolymers that show better optoelectronic properties to boost the PCE of polymer solar cells further. It is reported in literature that copolymers incorporating electron deficient 2,1,3-benzothiadiazole (BT) [9], thieono[3,4-b]-thiophene (TT) [10], thieno[3,4-c]pyrrole-4,6-dione (TPD) [11], and pyrrolo[3,4-c]pyrrole-1,4-dione (DPP) [12] derivatives show excellent absorption, and high carrier mobility, and consequently high PCE in both single and tandem PSCs. Among these BT analogue is considered a most promising acceptor unit, and copolymers incorporating BT unit gave a maximum PCE up to 8.2 % [9]. Many studies have shown that the photovoltaic properties of the D-A copolymers consist of BT acceptor can be tuned via the insertion/incorporation of electron donating or accepting units in BT moiety [13]. Among the various D-A conjugated copolymers, copolymers based on the combination of benzo[1,2-b:4,5-b']dithiophene (BDT) as the donor unit and 2,1,3-benzothiadiazole (BT) as the acceptor unit have widely used and demonstrated to be excellent photovoltaic performance. The BDT unit has symmetric has a symmetric and planar conjugated structure, which can easily recognize ordered π-π stacking and assist in charge transport ability.

Moreover, the BDT core provides two positions on the central benzene core for attaching the different substitutes to ensure the good solubility and tune the energy levels of the copolymers [8]. Wang successfully designed and synthesized a series of new benzothiadiazole based conjugated D-A copolymers and achieved a PCE of 8.3 % [9].

As discussed above, BDT and BT are the most commonly used electron donor and acceptors moieties used for the design of D-A copolymers. Therefore, conjugated D-A copolymers, denoted as P(BDT-DTBT) (in DTBT, two thiophene moieties are flanked into benzene ring of BT as a π-bridge for reducing steric hindrance and tuning the electrochemical energy levels) can be the ideal donor materials for high performance of PSCs. This combination is a kind of weak donor- strong acceptor copolymer [14]. The weak donor BDT helps maintain a low HOMO level and strong acceptor DTBT would reduce the bandgap of the resulting copolymer. It was reported that extending the fused ring system in the two dimension (2D) direction is expected to broaden the light absorption of the material with enhanced high energy bands. Moreover, the 2D conjugation would allow the delocalization of hole over the side chain, thus lowering the local charge density and coulombic interactions between the hole and the electron in the donor –acceptor interface [15].

Polymer solar cells based on conjugated copolymers containing imidazol unit exhibit a decent PCE of 4.1%. Flat structure of imidazol is covalently bonded with the polymer side chain increases the conjugation length and decrease the effective bandgap. Inspired by the distinct research papers, where imidazol derivatives are playing the role of acceptor fragments in the side chain of polymers, we synthesized new planar imidazol derivatives as weak donors structures, according to the concept of building of ideal conjugated copolymer "weak donor-strong acceptor" and inserted them in main polymer chain, in order to increase the effective length of conjugation and increase intramolecular charge transfer. We developed new thiophene-benzimidazol containing compounds with rigid planar structure and expected to decrease the bandgap due to the presence of thiophene-benzimidazol structures as weak donor fragments in the polymer main chain. These copolymers exhibit suitable HOMO energy level (optimal value of HOMO of the order of 5.4 eV), in order to achieve high value of open circuit voltage (V_{oc}) and relatively large values of LUMO energy level for effective charge transfer to PCBM. Inspired by the work reported in literature, we have designed three low bandgap D-A copolymers **P1**, **P2** and **P3** with different weak donors (fused thiophen-imidazol containing derivatives units) and same strong acceptor benzothiadiazole. These copolymer exhibit broad absorption profile extending from visible to near infrared region of

solar spectrum and low lying HOMO energy level, for achieving the high J_{sc} and V_{oc}. It is interesting that the device PCE was significantly increased from **P1**:$PC_{71}BM$ (4.55 %) to **P2**:$PC_{71}BM$ (5.16 %) and **P3**:$PC_{71}BM$ (6.76 %) after the optimization solvent additive. This indicates that solvent additive play an important role in enhancing the overall PCE of the polymer solar cells.

2. Experimental details

2.1 Instruments and characterization methods

^{1}H and ^{13}C NMR spectra of the starting compounds and copolymers were recorded on the spectrometer "Bruker Avance-400" with a working frequency of 400.13 and 100.62 MHz, respectively. IR spectra were recorded by a FT-IR spectrometer "Perkin-Elmer 1720-X", TGA and DSC analysis was performed on "Per-kin-Elmer TGA-7" and "Perkin-Elmer DSC 7" devices with heating rate of 20 deg/ min. The absorption spectra in the range 190–1100 nm were recorded on the spectrophotometer "Varian Cary 50." The source of the exciting light was a xenon lamp L8253, which is part of the block radiator with optical fiber output radiation "Hamamatsu LC-4." Cyclic voltammetry measurements were performed on a potentiostat-galvanostatm AUTOLAB Type III equipped with standard three-electrode scheme in an acetonitrile solution of 0.1 mol/L tributylammonium hexafluorophosphate (n Bu_4NPF_6) at a potential scan rate of 50 mV/s. Films of investigated polymers were deposited on a glass surface coated with ITO and then dried and used as working electrode. Ag/Ag+ and platinum were used as reference and counter electrodes, respectively.

2.2 Synthesis of monomers M1, M2, M3 and copolymers P1, P2 and P3: Detail of the synthesis of the monomers and copolymers is given in the supporting information

2.3 Device fabrication and characterization

The photovoltaic devices using copolymers as donor and $PC_{71}BM$ as acceptor were fabricated on the indium tin oxide (ITO) coated glass substrate as follow: The ITO coated glass substrates were cleaned continuously in ultrasonic baths containing acetone, detergent, de-ionized water and isopropanol. Then the cleaned ITO glass substrates were dried by high purity nitrogen gas and then treated by UV-ozone for 10 min. The solution of PEDOT:PSS (Clevios PVP Al 4093) was spin coated onto the cleaned ITO glass substrates at 2500 rpm for 30 sec and subsequently dried at 100° C for 20 minutes in air. The blends of **P1** or **P2** or **P3**:$PC_{71}BM$ of different weight ratios were prepared by dissolving the copolymers and fullerene derivatives in chloroform (CF) solution and stirring for about 2 h. For the solvent additive, i. e. DIO/CF, a small amount of DIO (3% by volume) is added to the CF solution.

The photoactive layer of **P1** or **P2** or **P3**:$PC_{71}BM$ (in different ratios i.e. 1:0.5, 1:1, 1:2 and 1:2.5 and CF with small amount of solvent additive DIO) was deposited onto the PEDOT:PSS layer by spin coating and then dried in ambient atmosphere. The optimized weight ratio is 1:2 and optimized solvent additive is 3 v%. Finally, an aluminum (Al) metal top electrode was deposited in vacuum on the active layer at a pressure of less than 10^{-5} Torr. The active area of the device was ca. 0.10 mm^2. The current density–voltage (J–V) characteristics were measured on a computer-controlled Keithley 236 source meter unit. A xenon lamp coupled with AM 1.5 optical filter was used as the light source, and the optical power at the sample was 100 mW/cm^2. The incident photon to current conversion efficiency (IPCE) of the devices was measured using a monochromator and xenon lamp as light source and resulting photocurrent was measured with source meter under short circuit condition.

3. Results and discussion

3.1 Synthesis of copolymers and characterization

In order to obtain new π-conjugated low bandgap thiophene –benzimidazol containing copolymers, we preliminary synthesized 5,8-dibromo-2-{4-[2 ethylhexyl)oxy] phenyl }-1-octyl-H-bisthieno[3,2-e:2',3'-g]benzimidazole **(M1)**, 5,8-dibromo-2-[5-(2 ethylhexyl)thiophene-2-yl]-1H-bisthieno[3,2-e:2',3'-g]benzimidazole **(M2)** and 5,8-dibromo-2-[1',1'2',2', 3',3', 4',4'-octafluorobutyl]-1H-bisthieno[3,2-e:2',3'-g]benzimidazole **(M3)** by direct cyclization of aromatic α-diketone (1) with hetaryl –substituted aldehides 2, 3 and 4 with the formation of imidazol cycle. In order to accomplish this the synthesis of different aryl- and hetaryl substituted aldehides 2, 3 and 4 containing branched substituents was made as reported in literature [16]. Then, by means of condensation of 2,7-dibromobenzo-[2,1-b:4,5-b']dithiophen-4,5-dione **1** with synthesized 4-(-2 ethylhexyloxy)benzaldehyde 2 and 5-(2-ethylhexyl)thiophene -2-carboxaldehyde **3** and **4** with ammonium acetate in acetic acid at boiling were obtained new compounds 5,8-dibromo-2-{4-[2 ethylhexyl)oxy]phenyl}-1H-bisthieno[3,2-e:2',3'-g]benzimidazole **(5)**, 5, 8- dibromo-2-[5-(2 ethylhexyl)thiophene-2-yl] -1H-bisthieno [3,2-e:2',3'-g] benzimidazole **(M2)** and 5,8-dibromo-2- [1',1'2',2',3',3,4',4'-octafluorobutyl]-1H-bisthieno[3,2-e:2'3'-g]benzimidazole **(M3)** with yield 74, 77 and 67 %, respectively as shown in Scheme 1. N-alkylation of compound 5 with octyiodide in the presence of K_2CO_3 gave the compound **M1** with the yield of 88 %. Alkyl substituents were introduced into donor molecules for increase of solubility of them and target co-polymeric materials in organic solvents.

The composition and structures of intermediate compounds, and also targeted monomers **M1**, **M2** and **M3** were confirmed by elemental analysis data, ^{1}H NMR and ^{13}C NMR spectroscopy (see the supporting information). In particular, in spectra ^{1}H NMR of monomer **M1** in weak field area in the range 8.07-7.05 ppm two singlets and two doublets are present which are related to protons of thiophene and phenyl units (Figure S1) . In strong field area at 4.43 and 3.95 ppm two resonate, typical for CH_2 group directly bonded to atom of nitrogen and oxygen. In the range 1.70-0.70 multiplets related to protons of alkyl units are shown. The ratio of integral intensities of aromatic part to aliphatic part well corresponds to the targeted structure of **M1**.

In ^{1}H NMR of **M2**, the singlet at 7.78 ppm corresponds to the proton of thiophene cycle, in proximity of benzene ring and at 6.90 and 7.80 two doublets, corresponding to protons of thiophene fragment, attached to the imidazol cycle. In strong field area at 2.90, the signal resonates typical for CH_2 group, directly connected to thiophene ring. In the range 1.20-0.70, the signals appear, typical for the rest 15 protons of aliphatic part of the monomer **M2** (Figure S2a). The ratio of integral intensities of aromatic part to aliphatic corresponds to the structure of **M2**. In the carbo spectrum of product **M2**, 18 signals are present, of which in the range 148.08-112.69 ppm seven resonances are present, corresponding to ternary atoms of carbon of heterocyclic and thiophene substituents. In the stronger field 42.41-11.23 ppm, 8 peaks appear related to 8 atoms of carbon of branched 2-ethylhexyl substituents of thiophene fragment (Figure S2b).

In proton spectra of **M3** in the range 13.50-6.50, three signals and one triplet are seen, related to the proton of imidazole cycle, thiophene fragment and octafluorobutyl fragment, respectively (Figure S3a). In ^{19}F NMR spectra of **M3**, four intensive signals are present, related to four couple equivalent atoms of fluorine (Figure S3b).

Obtained heteroaromatic thiophene-benzimidazol containing monomers **M1**, **M2**, and **M3** were used for the synthesis of new low bandgap D-A π- conjugated copolymers **P1**, **P2** and **P3** in the conditions of cross-coupling Stille reaction as shown in Scheme 2. Poly-condensation was carried out in the atmosphere of argon in toluene, using tetrakis(triphenylphosphine) palladium as a catalyst. The role of electron accepting component in the structures of **P1**, **P2** and **P3** copolymers is dithienobentheinodizole, weak electron donors fragments are monomers **M1**, **M2** and **M3**, respectively. Obtained polymers **P1**, **P2** and **P3** were purified from the residues of catalysts, tin-organic and low molecular impurities by two-fold re-sedimentation from solution in methanol and following extraction

with methanol, hexane and chloroform. Yield of polymer **P1**, **P2** and **P3** was 75-87%. The composition and structure of polymers **P1, P2** and **P3** were confirmed by elemental analysis data and ^{1}H NMR and ^{13}C NMR spectroscopy. In particularly, ^{1}H NMR spectra of **P2** (Figure S4) shows 6 aromatic protons of elementary chain are resonating in the range of 8.50-7.50 ppm. The signals of protons of aliphatic fragments are present in the range 2.50-0.50 ppm. The ratio of integral intensities of aromatic and aliphatic protons for copolymers **P1** and **P3** well corresponds to the proposed structures and confirms the appearance of the elemental chains on the macromolecules.

The thermal properties of the **P1, P2** and **P3** were investigated via DSC and TGA methods and the data were summarized in table 1. The glass transition temperature of **P1**, **P2** and **P3** estimated from DSC measurement are 185°, 200° and 195° C, respectively. All the copolymers have the sufficient high thermal stabilities. These results show that the copolymers show thermal stabilities sufficiently high for the use in polymer solar cells.

3.2 Optical and electrochemical properties

The normalized UV-visible absorption spectra of the three copolymers in chloroform solution and in thin film are shown in Figure 1a and 1b, respectively and corresponding data are summarized in Table 2. It can be seen from the Figure 1 and table 2 that both in solution and in the solid state, two main absorption bands are observed which is typical for D-A copolymers [17]. The absorption band in longer wavelength region comes from intramolecular charge transfer (ICT) between the donor and acceptor units, while the shorter wavelength band is attributed to the π-π* transition of the polymer main chain. Since all the polymers have same acceptor skeleton benzothiadiazole and different donor skeletons, the both absorption bands in shorter and longer wavelength regions are different due to the different polymer main chain and different ICT abilities. As for the longer wavelength bands, the absorption band of **P1** is blue shifted compared to **P2** and **P2** is blue shifted as compared to **P3**, which can be attributed to the different electron donating strength of electron donating units. In solution absorption peaks in longer wavelength regions are located at 608 nm, 514 nm and 645 nm, for **P1**, **P2** and **P3**, respectively which correspondingly redshifted to 638 nm, 524 nm and 670 nm for the spectra in thin film. These bathochromic shifts in absorption band in thin film as compared solution suggest a stronger interchain pi-pi stacking and a high degree of ordered arrangement in thin films. It was observed that only a minimal red-shift occurs for the absorption maximum of **P1** in going from solution to thin film. This may be attributed to the fact that the polymer chain aggregate somewhat in solution for **P1** because of

CF$_2$ substituents present in the backbone, imposing less barrier to the chain interacting compared to other copolymers. All the copolymers exhibit strong absorption ability in the wavelength range from 400 nm to 800 nm which is beneficial for harvesting of more sunlight and thus may lead to enhanced J$_{sc}$ in polymer solar cells. Compared to **P3**, **P2** exhibits significant blue shifts of the absorption maxima (ICT band) with 33 nm and 42 nm for solution and thin film, which may be due to the weaker electron ability of the benzene ring compared to the thiophene ring, resulting in decreased electron delocalization along the **P2** backbone. The optical bandgaps ((E_g^{opt}) estimated from the onsets of the thin film absorption spectra were 1.61 eV, 1.50 eV and 1.56 eV for **P1**, **P2** and **P3**, respectively.

Electrochemical properties of polymers were investigated using cyclic voltammetry. Cyclic voltammetry of polymer films was investigated in acetonitrile with 0.1M tetrabutylammonim perchlorate (Bu$_4$NCIO$_4$) at scan speed of 50 mV/s. Platinum electrode was used as the counter-electrode, Ag/Ag$^+$ in 0.1M solution of AgNO$_3$ as reference electrode, and Fc / Fc$^+$ as an external standard. The results of cyclic voltammograms are presented in Figure 2 and data were summarized in Table 2. Both the copolymers exhibit reversible or partly reversible redox properties. The HOMO and LUMO energy levels were calculated from their onset oxidation potential and onset reduction potentials according to the following expressions:

$$E_{HOMO} = -q(E_{onset}^{ox} + 4.48)eV$$
$$E_{LUMO} = -q(E_{onset}^{red} + 4.48)eV$$

The HOMO energy level of **P1, P2** and **P3** are -5.24 eV, -5.37 eV and -5.25 eV, respectively. The deeper HOMO energy level of all copolymers may helpful for achieving high open circuit voltage (V$_{oc}$) and air stability [18]. It is well known that the HOMO energy level of D-A copolymer is mainly governed by the electron donors [19], and therefore different HOMO levels are attributed to the different electron donor skeleton. The deeper HOMO energy level for **P2** as compared to other copolymers may be attributed thienyl unit present in the donor. Due to the twisting of the thienyl plane with the thiophen-imidazol plane, this conjugated plane act as weaker electron donor and gives rise to deeper HOMO energy level than **P1** and **P3** [20]. The LUMO levels of **P1, P2** and **P3** are -3.74 eV, -3.72 and -3.70 eV, respectively. The similar values of LUMO levels for these copolymers may attribute to the same acceptor skeleton. The LUMO offsets between the donor copolymers

8

and $PC_{71}BM$ (-4.1 eV) are larger than 0.3 eV, which is sufficient for effective exciton dissociation and charge transfer [21].

3.3 Photovoltaic properties

PSCs devices were fabricated to evaluate and compare the photovoltaic properties of these copolymers. We have used a commonly used device structure of $ITO/PEDOT:PSS/copolymer:PC_{71}BM/$ Al. The active layers of the devices were prepared by using DIO as solvent additive in chloroform as processing solvent. We have optimized the copolymer/$PC_{71}BM$ ratio and found the optimized ratio is 1:2 (w/w) for all **P1**, **P2** and **P3** blends with $PC_{71}BM$ and small amount of 1,8diiodooctane (DIO) (3 % v) was used to optimize the their photovoltaic performance. The concentration of DIO was varied from 1%, 2%, 3% and 4% and we found that 3 % is the optimal volume amount. We will discuss the results only for the optimum conditions.

Figure 3a displays the current –voltage (J-V) characteristics of the PSCs based on the **P1**, **P2** and **P3** as donor and $PC_{71}BM$ as acceptor. The corresponding photovoltaic data obtained from the J-V characteristics are complied in table 3. It can be seen from the Table 3 that device based on **P2** shows a V_{oc} of 0.92 V which is the highest one in the three types PSCs, which is attributed to the deeper HOMO level of **P2** (-5.37 eV) as compared to **P1** and **P3**. The similar value of V_{oc} for **P1** and **P3** is in good agreement with the similar values of their HOMO energy level. The devices based on **P1** and **P3** show J_{sc} values of 9.82 mA/cm^2 and 11.12 mA/cm^2, respectively, which are lower than that to the device of **P2** (11.48 mA/cm^2). The over all PCEs of the devices based on **P1** and **P3** are 4.55 % and 5.16 %, respectively which are much lower than that to the device based on **P2** (PCE = 6.76 %). The IPCE spectra of the devices are displayed in Figure 3b. It can be seen from this figure that the IPCE spectra of these three devices have different response range and similar to their absorption profiles, which covers the whole visible range up to 720 nm for **P2** and **P3** and 650 nm for **P1**. The device based on **P2** shows higher IPCE values than that to devices based on **P1** and **P2**, which is consistent with the J-V characteristics. Although the absorption band of **P2** is narrower than other two copolymers, but the IPCE spectra is broader than the absorption spectra of **P2**, may be attributed to the better nanomorphology of the **P2**:$PC_{71}BM$ blend as compared to other blends and the leads to the improved absorption in the longer wavelength regions and contributes to the photocurrent generation. Moreover, we have also estimated the values of Jsc from the integration of IPCE spectra and were about 9.68 mA/cm^2, 11.40 mA/cm2 and 11.02 mA/cm^2 for **P1**, **P2** and **P3** based BHJ polymer solar cells, which are very close to the values observed in J-V characteristics.

A important factor to control the J_{sc} is the crystallinity of the donor copolymer, because a high crystalline copolymer affords efficient charge carrier transport to the electrode after exciton dissociation. We measured the crystallinity of the copolymers blended with $PC_{71}BM$ by X-ray diffraction method and shown in Figure 4. The XRD pattern of the three copolymers reveals that **P1** and **P3** showed weaker diffraction peak of (100) as compared to **P2** indicating the **P2** has the highest crystallinity. In other words, the degree of crystallinity is of the order of **P2**, **P3** and **P1**. The improved crystallinity of **P2**:$PC_{71}BM$ as compared to other blends causes efficient charge transport.

We have measured the hole mobilities of the three copolymers blended with $PC_{71}BM$ by the standard method using a single carrier device to correlate crystallinity to the charge transport. The dark current-voltages characteristics in dark (log- log scale) were measured using a hole only device (ITO/PEDOT:PSS/copolymer:$PC_{71}BM$/Au) and shown in Figure 5 and shows straight lines with slope near to two, indicating the current is space charge limited (SCL). The voltage has been corrected as $V = V_{app} - V_{bi}$, where V_{bi} is the built in potential due to the difference in the work function of anode the cathode. We have achieved the SCLC region at quite lower voltages, may be attributed to the low value of thickness of active layer. The experimental data were fitted with SCLC model [22] (solid line in Figure 5) and hole mobility was estimated using the Mott-Gurney law and complied in table 3. We have also estimated the electron mobilities for all the blends using electron only device i.e. ITO/Al/copolymer:$PC_{71}BM$/Al and estimated values for all blends is about 2.36 $\times 10^{-4}$ cm^2/Vs. The increase in hole mobility from **P2** to **P3** and **P3** to **P1**, reduces the ratio between the electron and hole mobilities from 8.94 to 4.37 (**P3** to **P1**) and 4.37 to 3.05 (**P1** to **P2**), respectively, indicates a more balanced charge transport in the device based on **P2**:$PC_{71}BM$. The balance charge transport within the active layer resulted in high J_{sc} and FF.

The surface morphology properties of copolymers:$PC_{71}BM$ blend films were investigated using atomic force microscopy (AFM). The topography and phase images of copolymers: $PC_{71}BM$ prepared from DIO/CF solvent are shown in Figure 6. All the blended thin films showed different morphological properties. The mean square surface roughness of the films is 3.44 nm, 1.72 nm and 2.14 nm for **P1**:$PC_{71}BM$, **P2**:$PC_{71}BM$ and **P3**:$PC_{71}BM$ films, respectively. The phase images of these films are also exhibits different domain sizes, i.e. 38 nm, 18 nm and 22 nm, for **P1**:$PC_{71}BM$, **P2**:$PC_{71}BM$, and **P3**:$PC_{71}BM$, respectively. The domain size of **P1:**$PC_{71}BM$ is too large for efficient exciton dissociation; since the exciton diffusion length in most of the organic semiconductors is only 10-20 nm [22], thus the big domain size in the blend will cause strong germinate recombination.

We have estimated the maximum exciton generation rate (G_{max}) and exciton dissociation probability [P(E,T)] of the three blends according to the method reported in literature [24] and compared them to analyze the photovoltaic performance the devices. Figure 7 shows the variation of the photocurrent density (J_{ph}) with effective voltage (V_{eff}). Here $J_{ph} = J_L - J_D$, where J_L and J_D are the current density under illumination (100 mW/cm^2) and in dark conditions, respectively and $V_{eff} = V_o - V_{app}$, where V_o is the voltage at the point at which $J_{ph} = 0$, and V_{app} is the applied voltage. We assume that all of the photogenerated excitons are dissociated into free charge carriers at high V_{eff} due to sufficient electric field [25] and therefore, the G_{max} can be determined from the saturation current density (J_{sat}), i.e. $J_{sat} = qG_{max} L$, where q is the electronic charge and L is the thickness of the active layer. The value of G_{max} was estimated from Figure 7 and above expression and are 4.67 x10^{27} m^{-3}s^{-1}, 7.8 x10^{27}m^{-3}s^{-1} and 9.2 x10^{27}m^{-3}s^{-1}, for **P1**:PC$_{71}$BM, **P3**:PC$_{71}$BM and **P2**:PC$_{71}$BM based devices, respectively. This difference is probably due to the value of molar extinction coefficients and absorption profile of the blends. As the SB24 has broader absorption profile as compared to others, the higher value of Gmax for device based on **P2**:PC$_{71}$BM may be due to the broader absorption profile. We have also estimated the P(E,T), which is a function of electric field and temperature, using the relation $J_{ph} = qG_{max} P(E,T) L$, under short circuit conditions. The P(E,T) values of **P1**:PC$_{71}$BM, **P2**:PC$_{71}$BM and **P3**:PC$_{71}$BM under short circuit conditions are 72%, 85 % and 78%, respectively, suggesting that exciton dissociation probability is higher in the **P2**:PC$_{71}$BM than other two blends, which is attributed to the better nanophase morphology for this blend.

4. Conclusions

In this study, three low bandgap D-A conjugated copolymers **P1**, **P2** and **P3** based on different weak donor fused thiophen-imidazol containing derivatives units and same benzothiadiazole acceptor unit were synthesized by Stille cross- coupling polymerization and were characterized by ^{1}H NMR, elemental analysis and GPC, TGA, DSC. These copolymers exhibit broad absorption in visible and near infrared region of solar spectrum and low lying HOMO energy levels. Application of these copolymers as donor along with PC$_{71}$BM as acceptor in BHJ solar cells provide high V_{oc} and optimization of solar cells by solvent additive gave a PCE of 6.76 % for the device based on **P2** :PC$_{71}$BM active layer. These results show that the design of D-A copolymers with weaker donor and stronger acceptor structure is the excellent strategy for improvement in BHJ organic solar cells.
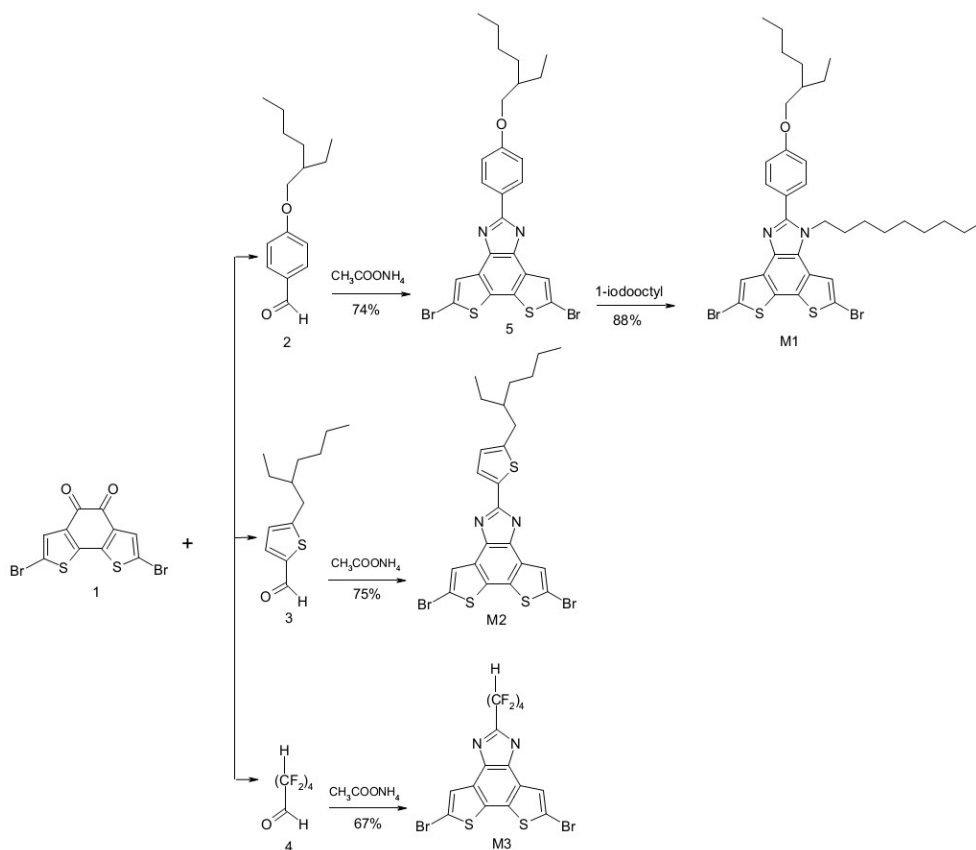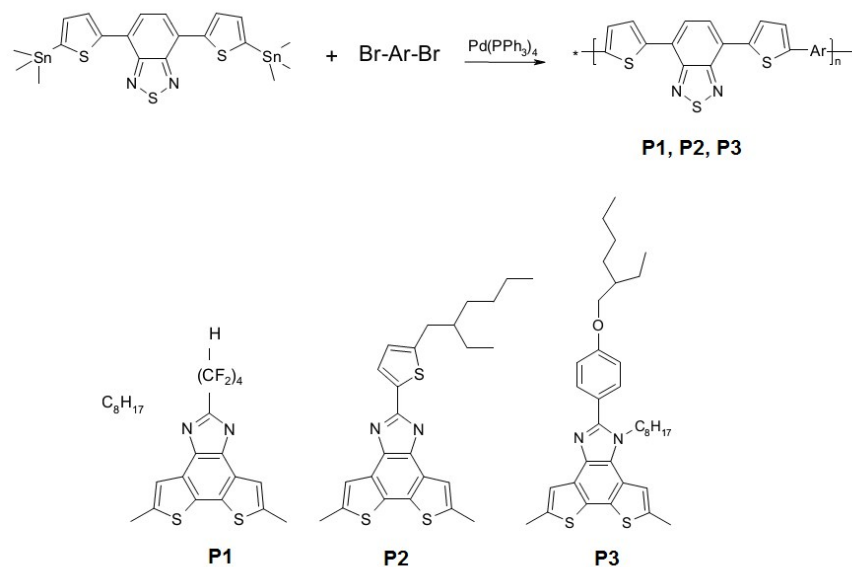
References

1. (a) I. Burgu´es-Ceballos, M. Stella, P. Lacharmoise and E. Mart´ınez-Ferrero, *J. Mater. Chem A* 2014, **2**, 17711; (b) E. Wang, W. Mammo and M. R. Andersson, *Adv. Mater*, 2014, **26**, 1801; (c) R. S. Kularatne, H. D. Magurudeniya, P. Sista, M. C. Biewer and M. C. Stefan, *J. Poly. Sci., Part A: Poly. Chem,* 2013, **51**, 743; (d) S.B. Darling and F. You, *RSC Advance*, 2013, 3, 17633; (e) W. Cao and J. Xue, *Energy Environ. Sci*, 2014, 7, 2123; (f) B. C. Thompson, P. P. Khlyabich, B. Burkhart, A. E. Aviles, A. Rudenko, G. V. Shultz, C. F. Ng and L. B. Mangubat, *Green* 2011, **1**, 29; (g) L. Ye, T. Xiao, N. Zhao, H. Xu, Y. Xiao, J. Xu, Y. Xiong and W. Xu, J. Mater. Chem.**,** 2012, **22**, 16723; (h) L. Ye, H. H. Xu, H. Yu, W. Y. Xu, H. Li, H. Wang, N. Zhao, and J. B. Xu, J. Phys. Chem. C, 2014, **118**, 20094; (i)L. Ye, H. Xia, Y. Xiao, J. Xu and Q. Miao, RSC Adv.**,** 2014, **4,** 1087

2. (a) G. Yu, J. Cao, J. C. Hummelen, F. Wudl and A. J. Heeger, *Science* 1995, **270**, 1789; (b) G. Li, V. Shrotriya, J. Huang, Y. Yao, T. Moriarty, K. Emery and Y. Yang, *Nat. Mater*, 2005, **4**, 864; (c) S. H. Park, A. Roy, S. Beaupré, S. Cho, N. Coates, J. S. Moon, D. Moses, M. Leclerc, K. Lee and A. J. Heeger, *Nat. Photon*, 2009, **3**, 297; (d) B. J. Moon, G-Y. Lee, M. J. Im, S. Song and T. Park, *Nanoscale* 2014, **6**, 2440

3. (a) Z. He, C. Zhong, S. Su, M. Xu, H. Wu and Y. Cao, *Nat. Photon*, 2012, **6**, 591; (b) S.-H. Liao, H.-J. Jhuo, Y.-S. Cheng and S.-A. Chen, *Adv. Mater*, 2013, **25**, 4766; (c) L. Ye, S. Zhang, W. Zhao, H. Yao and J. Hou, *Chem. Mater*, 2014, **26**, 3603

4. (a) http://www.nrel.gov/ncpv/images/effi_ciency_chart.jpg, (b) J. You, L. Dou, K. Yoshimura, T. Kato, K. Ohya, T. Moriarty, K. Emery, C.-C. Chen, J. Gao and G. Li, *Nat. Commun*, 2013, **4**, 1446

5. G. Dennler, M. C. Scharber, T. Ameri, P. Denk, K. Forberich, C. Waldauf and C. J. Brabec, *Adv. Mater*, 2008, **20**, 579

6. (a) S. Günes, H. Neugebauer and N. S. Sariciftci, *Chem. Rev*, 2007, **107**, 1324; (b) H. Hoppe and N. S. Sariciftci, *J. Mater. Res.* 2004, **19**, 1924; (c) G. Li, R. Zhu and Y. Yang, *Nat. Photon*, 2012, **6**, 153; (d) Z. He, C. Zhong, S. Su, M. Xu, H. Wu and Y. Cao, *Nat. Photon,* 2012, **6**, 591.

7. R. R. Lunt, T. P. Osedach, P. R. Brown, J. A. Rowehl and V. Bulovic*, Adv. Mater,* 2011, **23**, 5712

8. C. Gao, L. Wang, X. Li and H. Wang, *Polym. Chem,* 2014, **5**, 5200.

9. N. Wang, Z. Chen, W. Wei and Z. Jiang, *J. Am. Chem. Soc*, 2013,**135**, 17060.

10. Z. He, C. Zhong, S. Su, M. Xu, H. Wu and Y. Cao, *Nat. Photon*, 2012, **6**, 591.

11. C. Cabanetos, A. E. Labban, J. A. Bartelt, J. D. Douglas, W. R. Mateker, J. M. J. Frechet, M. D. McGehee and P. M. Beaujuge, *J. Am. Chem. Soc*, 2013, **135**, 4656.

12. (a) L. Dou, W.-H. Chang, J. Gao, C.-C. Chen, J. You and Y. Yang, *Adv. Mater*, 2013, **25**, 825; (b) L. Dou, J. Gao, E. Richard, J. You, C.-C. Chen, K. C. Cha, Y. He, G. Li and Y. Yang, *J. Am. Chem. Soc*, 2012, **134**, 10071.

13. (a) L. Fan, R. Cui, X. Guo, D. Qian, B. Qiu, J. Yuan, Y. Li, W. Huang, J. Yang, W. Liu, X. Xu, L. Li and Y. Zou, *J. Mater. Chem. C*, 2014, **2**, 5651; (b) M. L. Keshtov, D. V. Marochkin, V. S. Kochurov, A. R. Khokhlov, E. N. Koukaras and G. D. Sharma, *J. Mater. Chem. A*, 2014, **2**, 155; (c) L. Wang, D. Cai, Q. Zheng, C. Tang, S.-C. Chen and Z. Yin, ACS Macro Lett., 2013, **2**, 605; (d) G. Li, C. Kang, X. Gong, J. Zhang, W. Li, C. Li, H. Dong, W. Hub and Z. Bo, *J. Mater. Chem. C*, 2014, 2, 5116.

14. H. Zhou, L. Yang, W. You, *Macromolecules*, 2012, **45**, 607-632; (b) H. Zhou, L. Yang, S. Stoneking and W. You, *ACS Appl. Mater. Interfaces*, 2010, **2**, 1377.

15. (a) B. S. Rolczynski, J. M. Szarko, H. J. Son, Y. Liang, L. Yu and L. X. Chen, *J. Am. Chem. Soc*, 2012, **134**, 4142; (b) C. Risko, M. D. McGehee and J. L. Bredas, *Chem. Sci*, 2011, **2**, 1200; (c) S. S. Zade and M. Bendikov, *Angew. Chem., Int. Ed*, 2010, **49**, 4012.

16. B.C. Popere, A.M. Della Pelle and S. Thayumanavan, *Macromolecules* 2011, **44**, 4767-4776

17. Y. Zhang, J. Zou, C. C. Cheuh, H. L. Yip and A. K. Y. Jen, *Macromolecules*, 2012, **45**, 5427.

18. (a) B. C. Thompson, Y. G. Kim and J. R. Reynolds, Macromolecules, 2005, 38, 5359; (b) D. M. D. Leeuw, M. M. J. Simenon, A. R. Brown and R. E. F. Einerhand, Synth. Met., 1997, 87, 53, (c) M. L. Keshtov, D. V. Marochkin, V. S. Kochurov, A. R. Khokhlov, E. N. Koukaras and G. D. Sharma, Polym. Chem. 2014 4, 4033

19. Z. Ma, D. Dang, Z. Tang, D. Gedefaw, J. Bergqvist, W. Zhu, W. Mammo, M. R. Andersson, O. Inganäs, F. Zhang and E. Wang, *Adv. Energy Mater*, 2014, **4**, 1301455.

20. (a) L. J. Hou, J.H. Hou, S. Zhang, H.Y. Chen, Y. A. Yang, Amgew. Chem. Int. Ed. 2010, 49, 1500, (b) L.T. Dou, et al. Nat. Photonics 2012, 6, 180

21. (a) D. M¨ uhlbacher, M. Scharber, M. Morana, Z. Zhu, D. Waller, R. Gaudiana and C. Barbec, *Adv. Mater*, 2006, **18**, 2884; (b) A. P. Zoombelt, M. Fonrodona, M. G. R. Turbiez, M. M. Wienk and R. A. J. Janssen, *J. Mater. Chem*, 2009, **19**, 5336; (c) J. Y.

Kim, K. Lee, N. E. Coates, D. Moses, T.-Q. Nguyen, M. Dante and A. J. Heeger, *Science*, 2007, **317**, 222.

22. (a) C. Meizer, E.J. Koop, V.D. Mihailetchi and P.W.M. Blom, *Adv. Funct. Mater*, 2004, **14**, 865; (b) V.D. Mihailetchi, L.J.A. Koster, P.W.M. Blom, C. Meizer, D. de Boer, J.K.J. VanDuren and R.A.J. Janssen, *Adv. Funct. Mater*, 2005, **15**, 795.

23. T. M. Clarke and J.R. Durrant, *Chem. Rev*, 2010, **110**, 6736.

24. (a) J.-L. Wu, F.-C. Chen, Y.-S. Hsiao, F.-C. Chien, P. Chen, C.-H. Kuo, M. H. Huang and C.-S. Hsu, *ACS Nano*, 2011, **5**, 959; (b) L. Lu, Z. Luo, T. Xu and L. Yu, *Nano Lett*, 2013, **13**, 59.

25. V. D. Mihailetchi, L. J. A. Koster, J. C. Hummelen and P. W. M. Blom, *Phys. Rev. Lett*, 2004, **93**, 216601.

Scheme 1 synthesis of **M1**, **M2** and **M3** monomers

Scheme 2. Synthesis of **P1**, **P2** and **P3** D-A copolymers

Table 1. Molecular weights and Thermal Properties of copolymers **P1, P2** and **P3**.

Copolymer	Yield (%)	M_n^a (kgmol^{-1})	M_w (kgmol^{-1})	PDI	T_g^b (°C)	T_d^c (°C)
P1	75	12 .8	24.8	1.94	185	384 387
P2	81	13.9	29.6	2.13	200	387 406
P3	87	15.4	35.6	2.31	195	379 398

[a]Determined by GPC in THF on polystyrene standards.
[b] Determined by DSC at scan rate 20°C/min under nitrogen.
[c] Decomposition temperature, determined by TGA in nitrogen based on 5% weight loss, in numerator – temperature of 5% mass loss in air, in denominator – numerator 5% mass loss in Argon atmosphere

Table 2.Optical and Electrochemical Properties of copolymers **P1, P2** and **P3**

Polymer	λ_{max}^{abs} (nm),solv	λ_{max}^{abs} (nm),film	E_{onset}^{ox} (V)	HOMO (eV)	E_{onset}^{red} (V)	LUMO (eV)	E_g^{ox} (eV)	E_g^{opt} (eV)
P1	393, 604	397, 640	0.76	-5.24	-0.74	-3.74	1.50	1.61
P2	379, 516	379, 524	0.89	-5.37	-0.76	-3.72	1.65	1.50
P3	432, 645	437,670	0.77	-5.25	-0.70	-3.78	1.47	1.56

Table 3 Photovoltaic parameters of polymer solar cells fabricated with **P1**, **P2** and **P3** as donor and $PC_{71}BM$ as acceptor processed with chloroform and 3 % v DIO

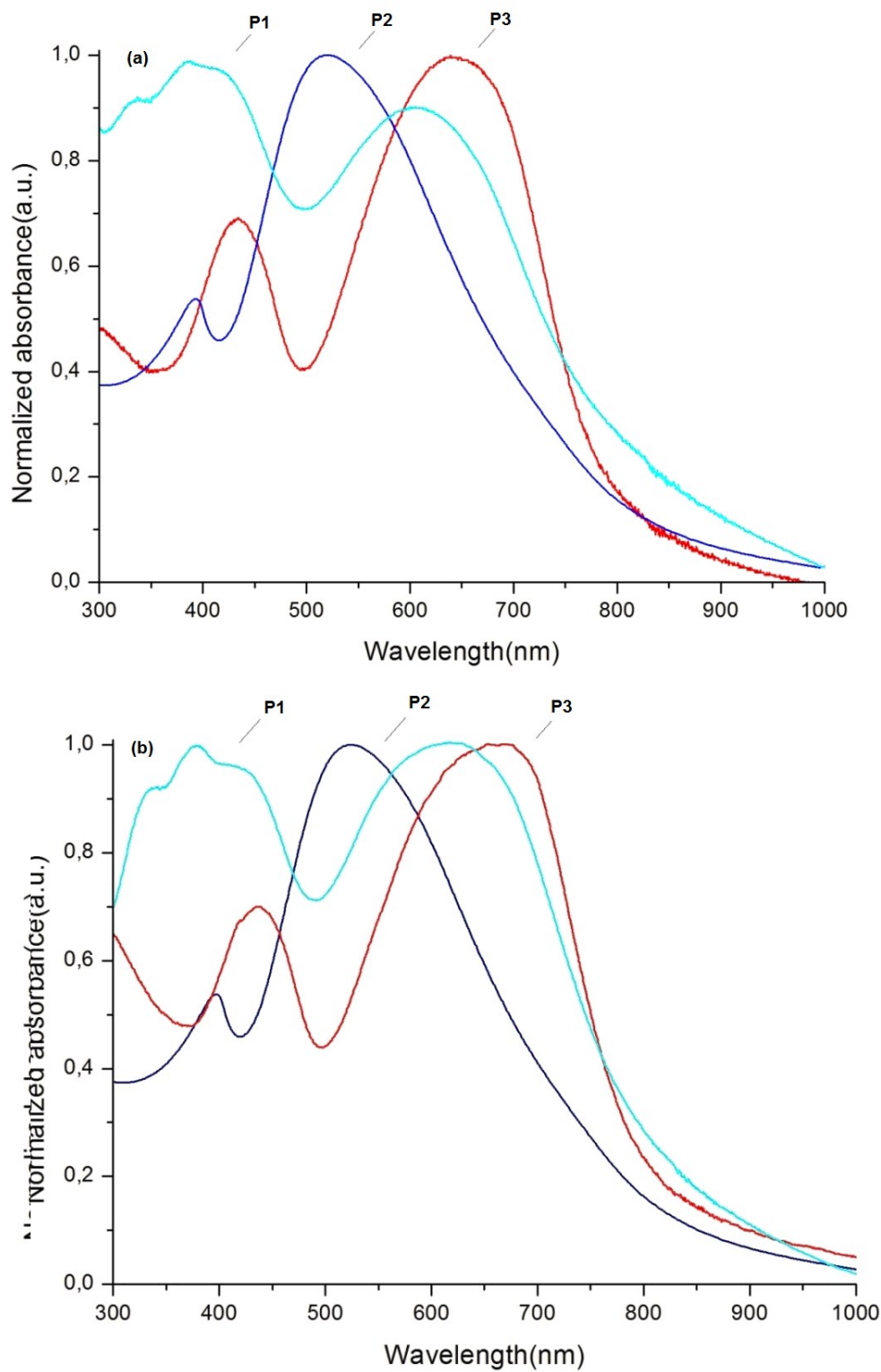| Blend	J_{sc} (mA/cm^2)	V_{oc} (V)	FF	PCE (%)	μ_h (cm^2/Vs)	μ_e/μ_h
P1:$PC_{71}BM$	9.82	0.80	0.58	4.55	2.64 x10^{-5}	8.94
P2:$PC_{71}BM$	11.48	0.92	0.64	6.76	7.74x10^{-5}	4.37
P3:$PC_{71}BM$	11.12	0.80	0.58	5.16	5.42x10^{-5}	3.05

16

Figure 1. Normalized absorption spectra of copolymers **P1**, **P2** and **P3** in (a) solution and (b) thin film prepared for chloroform solution
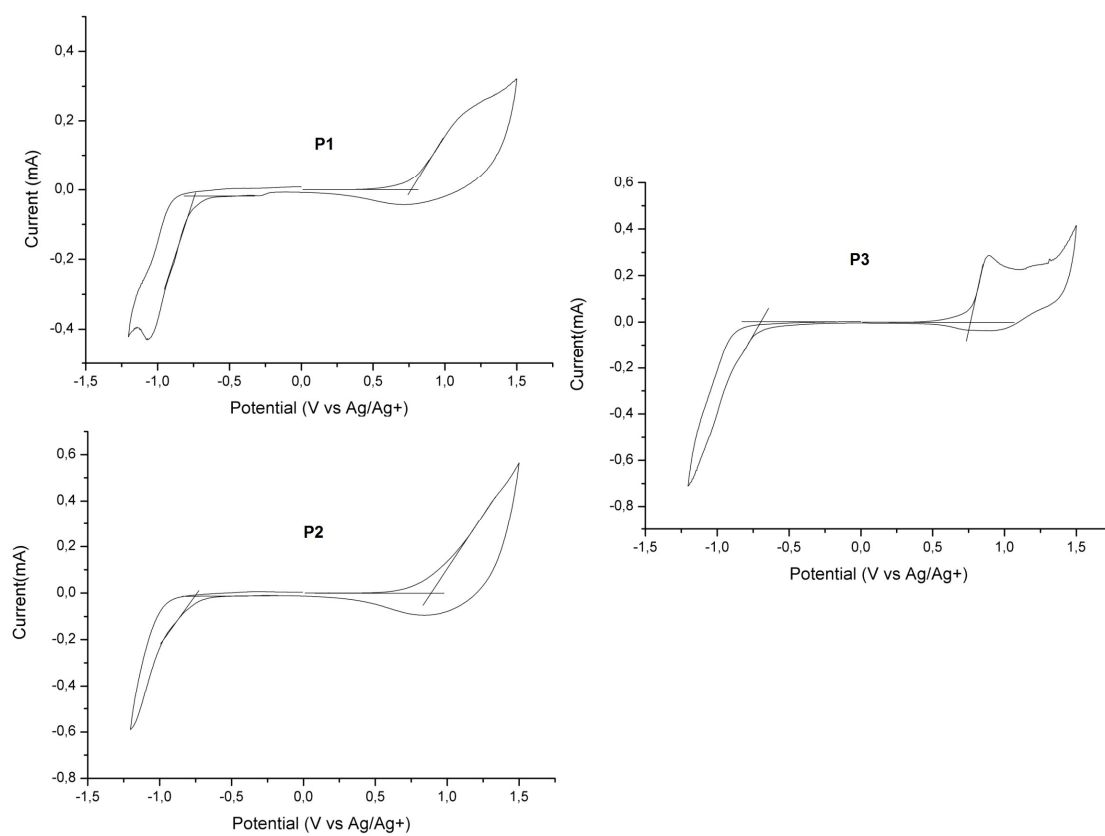
Figure 2. Cyclic voltammetry curves of copolymers **P1**, **P2** and **P3** films on platinum electrode in 0.1 mol/L Bu$_4$NClO$_4$ in CH$_3$CN solution at scan rate of 50 mV/S
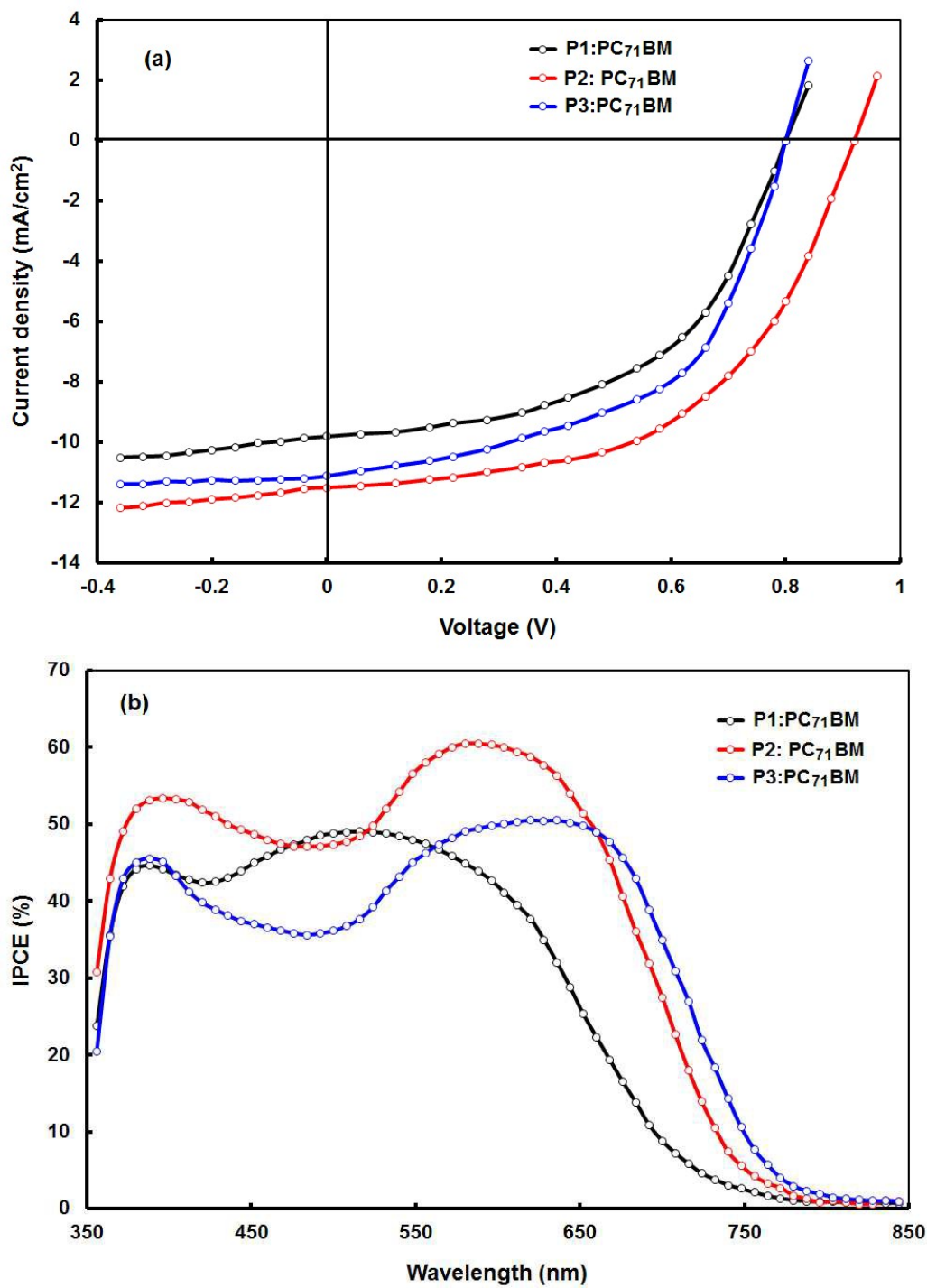
Figure 3. (a) Current –voltage (J-V) characteristics under illumination (100 mW/cm^2) and (b) IPCE spectra of copolymer:PC$_{71}$BM BHJ polymer solar cells
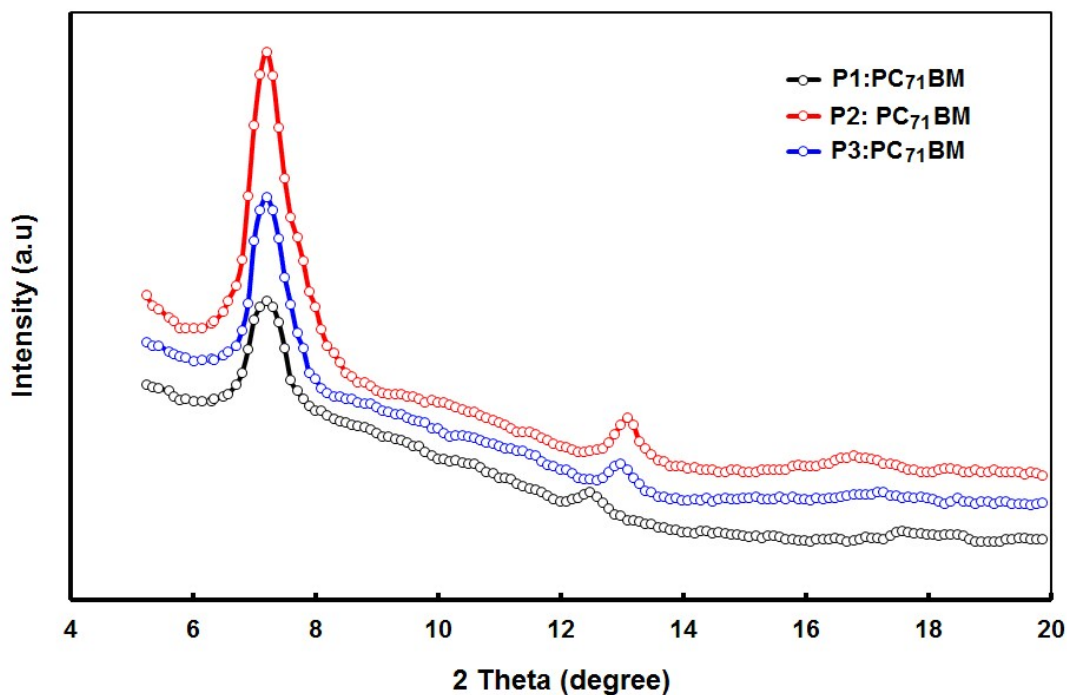
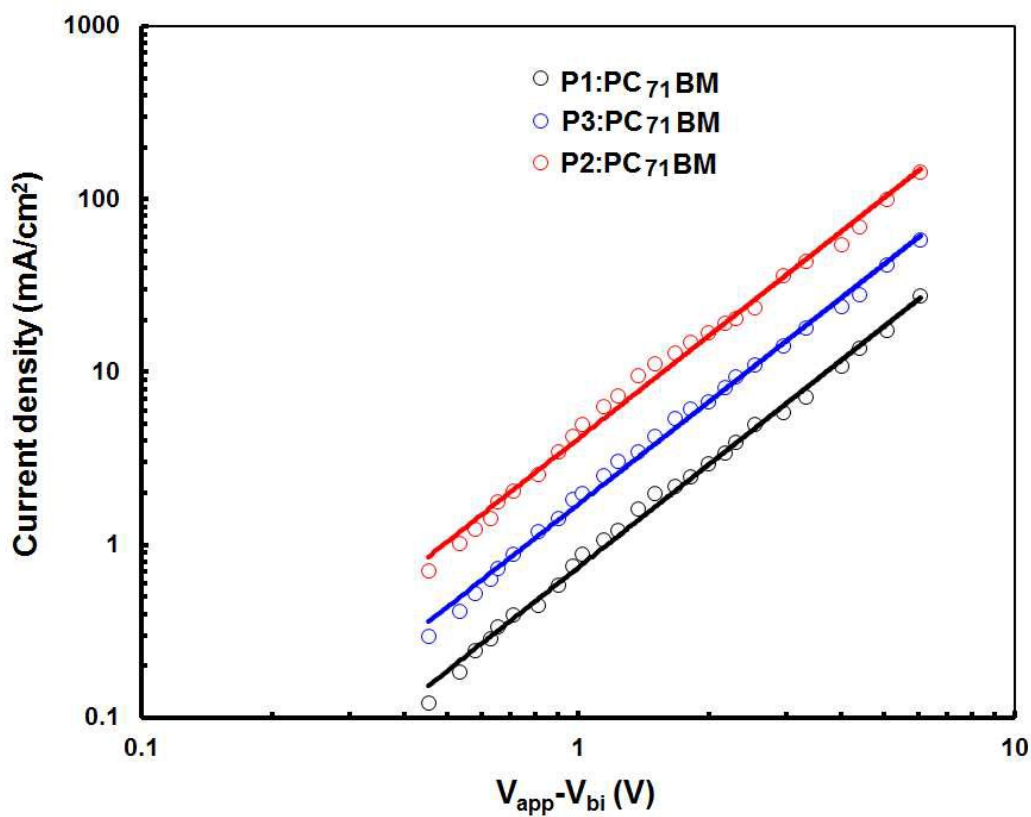Figure 4. XRD patterns of the blends cast from DIO/CF solvent

Figure 5. Dark current –voltage (J-V) characteristics of copolymer:$PC_{71}BM$ blends for hole only devices, solid lines are SCLC fitting.
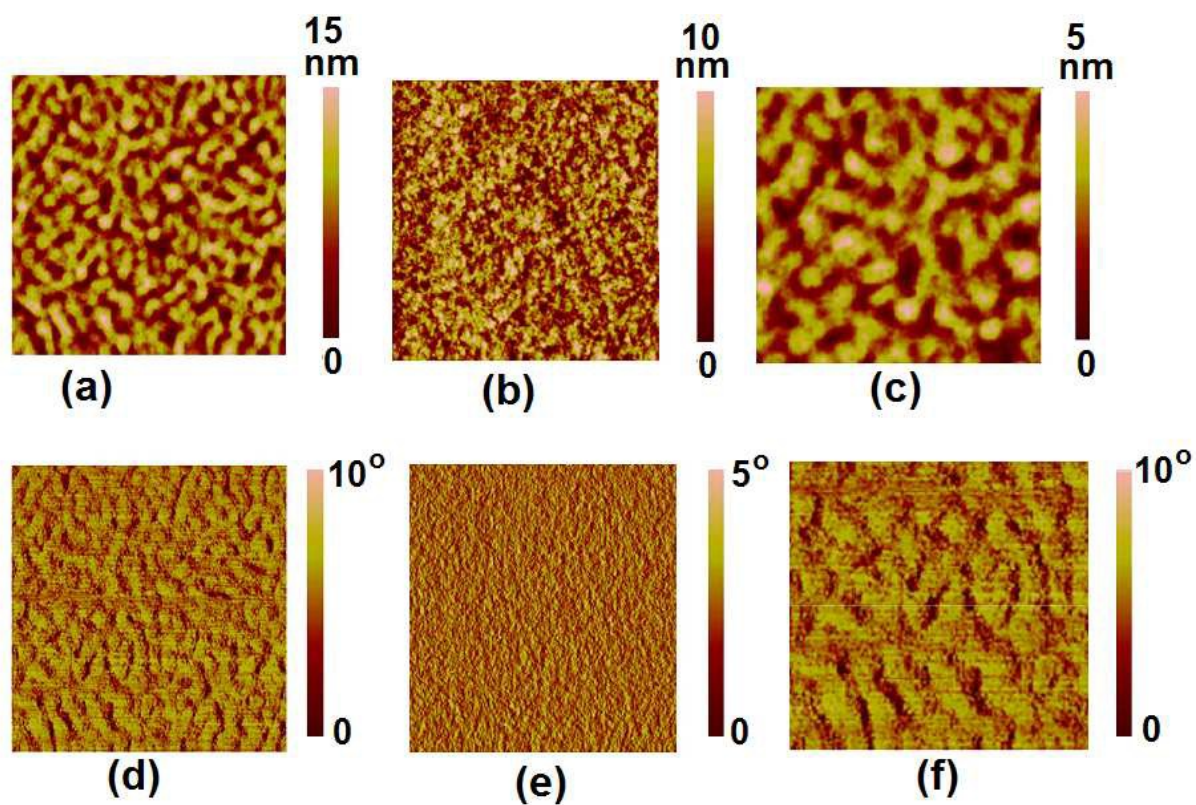
Figure 6. Tapping-mode AFM images: topography image and phase image of the blend films of **P1**:PC$_{71}$BM (a, d), **P2**:PC$_{71}$BM (b, e), and **P3**:PC$_{71}$ BM (c, f) processed with CF and 3% (v/v) DIO. AFM image sizes are 3μm x3 μm.
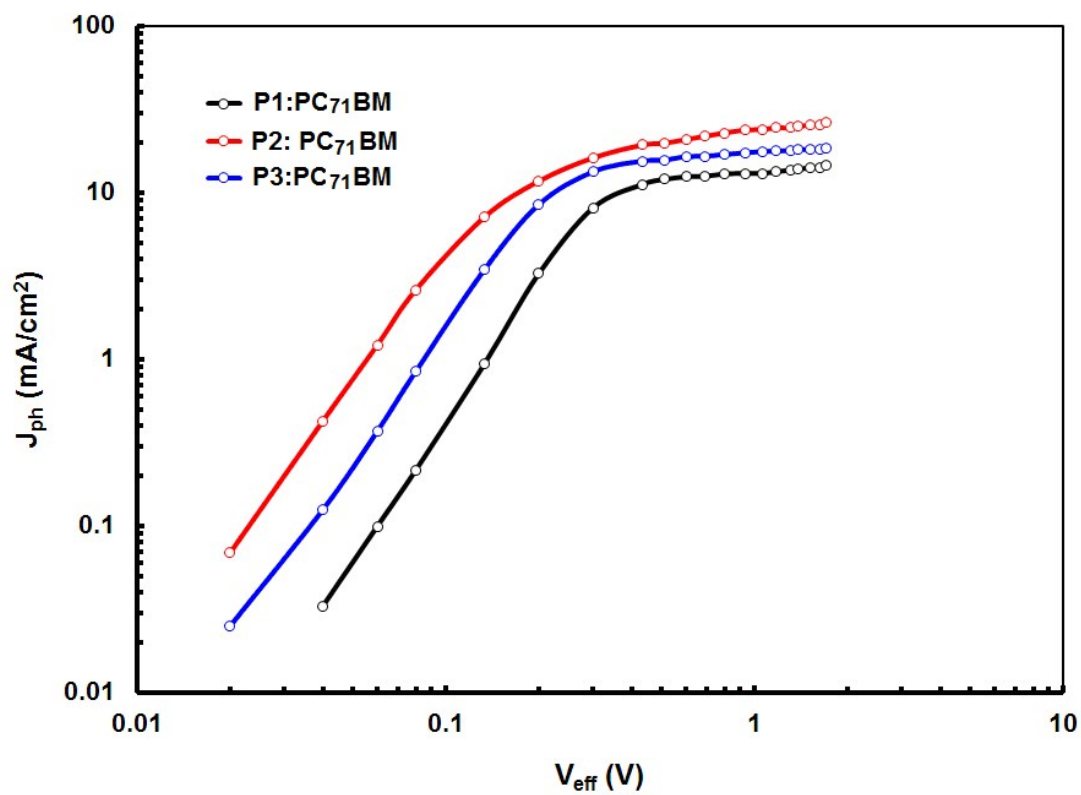
Figure 7. Variation of photocurrent density (J_{ph}) with effective voltage (V_{eff}) for the devices